Cellular/Molecular

Transient and Sustained Ganglion Cell Light Responses Are Differentially Modulated by Intrinsically Produced Reactive Oxygen Species Acting upon Specific Voltage-Gated Na$^+$ Channel Isoforms

Benjamin J. Smith,[1,2] Cyrus F. McHugh,[1] Arlene A. Hirano,[2] Nicholas C. Brecha,[2,3,4,5,6] and Steven Barnes[1,2,3]

[1]Doheny Eye Institute, University of California, Los Angeles, California 91103, [2]Department of Neurobiology, David Geffen School of Medicine, University of California, Los Angeles, Los Angeles, California 90095, [3]Department of Ophthalmology, David Geffen School of Medicine, University of California, Los Angeles, Los Angeles, California 90095, [4]Veterans Administration Greater Los Angeles Healthcare System, Los Angeles, California 90073, [5]Department of Medicine, David Geffen School of Medicine, University of California, Los Angeles, Los Angeles, California 90095, and [6]Stein Eye Institute, David Geffen School of Medicine, University of California, Los Angeles, Los Angeles, California 90095

Increasing spike rates drive greater neuronal energy demand. In turn, mitochondrial ATP production leads to the generation of reactive oxygen species (ROS) that can modulate ion channel gating. Does ROS production autoregulate the excitability of a neuron? We investigated the links between retinal ganglion cell (RGC) excitability and spike activity-driven ROS production in male and female mice. Changes to the light-evoked and current-evoked spike patterns of functionally identified αRGC subtypes, along with their Na$_V$ channel-gating properties, were recorded during experimentally induced decreases and increases of intracellular ROS. During periods of highest spike rates (e.g., following light onset in ON sustained RGCs and light offset in OFF sustained RGCs), these αRGC subtypes responded to reductions of ROS (induced by catalase or glutathione monoethyl ester) with higher spike rates. Increases in ROS (induced by mercaptosuccinate, antimycin-A, or H$_2$O$_2$) lowered spike rates. In ON and OFF transient RGCs, there were no changes in spike rate during ROS decreases but increased ROS increased spiking. This suggests that endogenous ROS are intrinsic neuromodulators in RGCs having high metabolic demands but not in RGCs with lower energy needs. We identified ROS-induced shifts in the voltage-dependent gating of specific isoforms of Na$_V$ channels that account for the modulation of ON and OFF sustained RGC spike frequency by ROS-mediated feedback. ROS-induced changes to Na$_V$ channel gating, affecting activation and inactivation kinetics, are consistent with the differing spike pattern alterations observed in RGC subtypes. Cell-autonomous generation of ROS during spiking contributes to tuning the spike patterns of RGCs.

Key words: action potential; ganglion cell; reactive oxygen species; retina; RGC; sodium channel

---

Significance Statement

Energy production within retinal ganglion cells (RGCs) is accompanied by metabolic by-products harmful to cellular function. How these by-products modulate the excitability of RGCs bears heavily on visual function and the etiology of optic neuropathies. A novel hypothesis of how RGC metabolism can produce automodulation of electrical signaling was tested by identifying the characteristics and biophysical origins of changes to the excitability of RGCs caused by oxidizing by-products in the retina. This impacts our understanding of the pathophysiology of RGC dysfunction, supporting an emerging model in which increases in oxidizing chemical species during energy production, but not necessarily bioenergetic failure, lead to preferential degeneration of specific subtypes of RGCs, yielding loss of different aspects of visual capacity.

Introduction

To convey visual information to the brain, retinal ganglion cells (RGCs) generate action potentials that traverse long sections of unmyelinated axon across the retinal surface before entering the optic nerve. Maintaining the transmembrane ionic gradients required for signaling with action potentials in unmyelinated nerves requires great expenditure of ATP. Inherited and environmental optic neuropathies often involve mitochondrial proteins and despite their ubiquitous expression in all neurons, RGCs are preferentially lost, underscoring the constraints imposed by metabolism on RGC function. RGC subtypes have unique biophysical properties (O'Brien et al., 2002; Margolis and Detwiler, 2007; Wong et al., 2012), which vary considerably between the subtypes (Emanuel et al., 2017; Werginz et al., 2020). While the ion channel properties of RGCs have been investigated using patch-clamp analysis of isolated cells (Lukasiewicz and Werblin, 1988), no reports describe the ion channel complement and voltage-dependent kinetics that determine the unique electrogenic phenotypes of RGC subtypes *in situ*. A theoretical framework, metabolically efficient coding (Crotty et al., 2006), seeks to explain the evolutionary constraints that shape the diverse electrogenic phenotypes of different neuronal subtypes, proposing that keeping metabolic expense under control constrains the biophysical properties of neurons in the trade-off between bandwidth (spike rate) and energetic cost (Carter and Bean, 2009; Hasenstaub et al., 2010). "Brisk" αRGCs provide high-bandwidth channels, whereas most RGCs spike at low frequencies (Koch et al., 2004, 2006), below maximal information transfer rates.

Metabolic by-products, including reactive oxygen species (ROS) produced when mitochondria generate ATP, are potent neuromodulators (Lee et al., 2015), altering biophysical factors including neurotransmitter-gated and voltage-gated channels. Prolonged periods of increased spiking raise ROS levels (Avshalumov et al., 2005). Oxidants target multiple proteins involved in neuronal excitability including GABA receptors (Accardi et al., 2014), TRP channels (Chuang and Lin, 2009), voltage-gated Na_V (Evans and Bielefeldt, 2000; Kassmann et al., 2008), Ca_V (Li et al., 1998), and K_V channels (Dantzler et al., 2019), and ATP-gated K^+ channels (Avshalumov et al., 2005). Even within ion channel classes, such as the Na_V classes, oxidant effects differ considerably between molecular isoforms (Kassmann et al., 2008; Schlüter and Leffler, 2016), complicating predictions of how ROS affect neuronal function.

RGCs are broadly categorized by the kinetics (sustained vs transient) and polarity (ON vs OFF) of their light responses. Sustained subtypes produce tonic spiking during light responses while transient cells spike phasically in response to light onset or offset. Analysis of mouse RGCs shows ~17 sustained and ~16 transient subtypes (Goetz et al., 2022). Sustained αRGCs have high basal activity levels and thus high metabolic demand, while transient cells produce sparse responses with lower metabolic demand. In mice, αRGCs comprise four cell types divided into ON and OFF sustained and ON and OFF transient subtypes (Krieger et al., 2017), which produce high spike rates and have fast axonal conduction velocities.

The investigations reported here tested the hypothesis that the elevated spike rates of sustained αRGCs, but not transient αRGCs, increase metabolic demand producing greater ROS production, and that increased ROS levels then act as feedback signals to slow spiking. Light stimulation of identified αRGC subtypes with experimentally enhanced intracellular ROS scavenging or artificially increased ROS, permitted the characterization of changes in light-evoked spike patterns. The results suggest that ROS act intrinsically to modulate responses to light in RGCs during tonically elevated metabolic demand. The data also show that Na_V1.1/1.3 channels, which facilitate sustained spiking in response to light, are more susceptible to modulation by ROS leading to reduced spiking. This evidence suggests that Na_V channel subtypes responsible for continuous, rapid spiking in sustained cells are the ones most sensitive to ROS, enabling both lasting high spike rates and an automatic reduction of spike rate when ROS levels become excessive. This may reflect an evolutionary solution that actively guards the most energy stressed RGCs against high levels of ROS, triggered when the RGCs produce elevated ATP and ROS during periods of high energy demand.

Materials and Methods

Patch-clamp recording of dark-adapted RGCs in isolated mouse retina. Experiments were performed using genetically labeled mouse αRGCs in accordance with the ARVO (The Association for Research in Vision and Ophthalmology) "Statement for the Use of Animals in Ophthalmic and Vision Research" and with the guidelines for the welfare of experimental animals issued by the US Public Health Service "Policy on Human Care and Use of Laboratory Animals" (2002). All recordings of light-induced and current-induced responses, as well as voltage-clamp analysis of Na_V channel currents, were made using the *Kcng4-cre::tdTomato* mouse line (Krieger et al., 2017). A subset of experiments tested the light responsivity of type 1 melanopsin-containing, intrinsically photosensitive RGCs from the OPN4^{EGFP} mouse line (MRRC#033064-UCD; Matynia et al., 2016). Male and female mice were deeply anesthetized with 1–3% isoflurane (IsoFlo, Abbott Laboratories) and decapitated. The eyes were then enucleated in dim light, and the anterior portion including the lens was removed. The resulting eyecup was trimmed, and a section of retina placed vitreal side up in a superfusion chamber was mounted on the microscope. These flat-mounts typically included a layer of full or partial pigmented epithelial cells under the photoreceptor layer. Retinas were superfused via a gravity driven fast flow system (ALA) with a bath solution containing the following (in mM): 120 NaCl, 2 CaCl$_2$, 3 KCl, 1 MgCl$_2$, 1.2 NaH$_2$PO$_4$, 10 glucose, and 25 NaHCO$_3$, bubbled continuously with 95% O$_2$/5% CO$_2$ and maintained at 34°C with an inline feedback-regulated heater (ALA). This was preferred over other commonly used solutions, such as the Ames test, that contain ingredients having significant redox-regulating properties.

Patch electrodes with 2–8 MΩ open tip resistance were pulled from fire-polished borosilicate glass capillary tubes using a micropipette puller (Sutter Instrument). The bath reference electrode consisted of an AgCl wire in a side chamber. Cell voltage was clamped with an amplifier (MultiClamp 700B, Molecular Devices) using whole-cell capacitance and series resistance compensation. Current signals were filtered at 5 kHz and digitized at 10 kHz with a digitizer (Digidata 1440A, Molecular Devices) for storage on the hard disk of a computer running pCLAMP 9 acquisition software (Molecular Devices). Patch pipettes were filled with the following (in mM): 10 KCl, 120 K-gluconate, 0.5 CaCl$_2$, 5 EGTA, 10 HEPES, 4 Mg-ATP, 0.4 lithium-GTP, and 10 phosphocreatine, and buffered to pH 7.2. Recordings using the *Kcng4-cre::tdTomato* line fit the established αRGC electrophysiological statistics and structural features of large somata and stout axons (Peichl, 1991; Krieger et al., 2017). The tdTomato-expressing type 5 bipolar and displaced amacrine cells were easily identified, and recording from them was avoided. Difficulties involving space clamp (e.g., voltage clamp of all cellular compartments, including the long RGC axon) hinder the study of large and fast voltage-gated currents in intact RGCs, and since acutely isolated RGCs, where space clamp is optimized, cannot be identified by their light response, we used the outside-out nucleated patch technique in identified, light-responsive RGCs in the *ex vivo* flat-mount retinal preparation (Lipton and Tauck, 1987). Nucleated patch recordings used a pipette solution containing the following (in mM): 120 CsMeSO$_4$, 2.8 NaCl, 0.3 CaCl$_2$, 5 EGTA, 20 TEACl, 2 Mg-ATP, 0.5 Na$_3$-GTP, 10 HEPES, and 10 Na$_2$-phosphocreatine, at pH 7.3. Nucleated patches were

corrected for a measured liquid junction potential of -7.5 mV. Series resistance was compensated by 70–100%.

Patch-clamp recordings were made using infrared light for cell visualization to maintain dark-adapted conditions, and td-Tomato-expressing RGCs were identified with one to two brief fluorescence-evoking green light steps ($\sim$500 ms). Once a cell was targeted, a dark waiting period of 5–10 min was observed before patching the cell under infrared illumination to minimize any light adaptation effects. Green light steps (530 ± 10 nm; SOLA TRITC emission, Nikon) were then applied to determine whether the αRGC was sustained or transient and ON or OFF type. Light steps had a stimulus intensity at 530 nm of 5.12×10^6 photons/μm^2/s corresponding to 2.26×10^6 R*/rod/s assuming a light-collecting area for mouse rods of $0.63 \mu m^2$ (Smeds et al., 2019) and using the mouse rhodopsin absorbance spectrum (Wang et al., 2011). This stimulus corresponded to 7.37×10^5 isomerization/M cone opsin/cone/s, assuming a collecting area of $0.12 \mu m^2$ (Sakurai et al., 2011). Testing the effects of endogenous ROS level changes on RGC excitability was done with current-clamp recordings of spontaneous, light-evoked, and current-evoked spiking while (1) reducing normal levels of ROS by adding catalase (2000–5,000 U/mg protein; diluted to 200–500 IU/ml; catalog #C1345, Sigma-Aldrich) after solubilization, to the pipette solution; (2) increasing ROS level by adding antimycin-A (2 μM; catalog #A8674, Sigma-Aldrich) to the pipette solution; or (3) reversibly increasing ROS levels in the entire retina using mercaptosuccinate (MCS; 1 mM; catalog #88460, Sigma-Aldrich) in the superfusion solution or with nonreversible puff applications of glutathione monoethyl ester (GME; catalog #G1404, Sigma-Aldrich) or H_2O_2 (100 μM; catalog #H1009, Sigma-Aldrich) near the cell soma (Avshalumov et al., 2005). ROS increases during voltage-clamp recordings of Na_V channels used short puffs of H_2O_2. Sodium channels were blocked with tetrodotoxin (TTX; 1 μM; catalog #T8024, Sigma-Aldrich) or the Na_V1.1/1.3 subtype-specific blocker ICA121431 (500 nM; catalog #5066, Tocris Bioscience).

Experimental design and statistical analysis. All data are reported as the mean $\pm$ SEM. Data were analyzed using Clampfit 10.3 (Molecular Devices). Graphing and statistical analyses were performed using MATLAB (MathWorks), Python 3.7, R (University of Vienna), and/or Excel (Microsoft). Statistical significance was tested with paired t tests, or when more than two treatments were involved, ANOVA with *post hoc* Tukey's HSD test. Spike properties (see Figs. 6, 10) were tested for significance using nonparametric tests including the Mann–Whitney U test or the Kruskal–Wallis test with *post hoc* Dunn's test if more than two treatments were involved. This was because of significant bimodality in the experimental outcomes. The statistics program R only reported up to approximately $p < 10^{-10}$ with high n values; hence, this value is shown in these cases, otherwise we denote p values as the actual computed value with values of <0.05 considered to be statistically significant and are denoted in the figures with one asterisk, while $p < 0.01$ and $p < 0.001$ are denoted with two and three asterisks, respectively.

Results

Changes to spiking in RGCs occur in response to elevated natural oxidizing species levels

Light-evoked spiking drives rapid metabolic demand and reveals that different RGC subtypes consume energy at very different rates (Perge et al., 2009). We investigated whether metabolic byproducts might act intrinsically to modulate RGC spiking and whether such effects might depend on the basal metabolic demand on the cell. *Kcng4-cre::tdTomato* mice (Krieger et al., 2017) were used since these mice have four types of fluorescently labeled RGCs that can be divided by the average spike rate, and thus metabolic demand, both during spontaneous and light-evoked activity. ON and OFF sustained cells have relatively high levels of spontaneous activity and spike for the entire duration of their preferred light stimulus. ON and OFF transient cells have relatively low levels of spontaneous activity and spike only for a brief duration to their preferred stimulus.

By blocking glutathione peroxidase, which degrades low concentrations of free H_2O_2 to water, with MCS; (1 mM), the resulting increase in cytoplasmic H_2O_2 produced strikingly different effects in sustained and transient αRGCs stimulated by 1.2 s light steps, and the changes in spiking could generally be reversed on washout of MCS (Fig. 1). In ON transient cells (Fig. 1B), MCS addition significantly increased the maximum spike rate ($142 \pm 13\%$ of control, $p = 0.038$, $n = 8$) and the number of spikes during the light response ($121.7 \pm 39\%$ of control, $p = 0.009$), while in ON sustained RGCs (Fig. 1A) both metrics were significantly reduced (maximum spike rate: $51 \pm 7\%$ of control, $p = 9.2 \times 10^{-6}$; number of spikes: $53 \pm 1\%$ of control, $p = 0.007$, $n = 8$) with responses becoming much more transient in nature. This general trend was also observed in OFF sustained cells, albeit to a lesser degree, as only the number of spikes was reduced (Fig. 1C; $55 \pm 1\%$ of control $p = 0.01$, $n = 9$), and no effect was observed in OFF transient cells (Fig. 1D). Two more non-αRGC types were tested to evaluate the generality of this trend: M1 intrinsically photosensitive RGCs, with high levels of spontaneous activity and prolonged light responses; and unlabeled ON-OFF transient cells targeted using their large soma size. Light-evoked spiking in M1 cells was strongly reduced by MCS (Fig. 1E; spike rate: $15 \pm 4\%$ reduction, $p = 1.7 \times 10^{-5}$; spike number: $35 \pm 9\%$ reduction, $p = 0.0006$, $n = 12$), although in these cells recovery postwash was not observed. ON-OFF transient cells showed an increase in excitability during the ON component of the response (Fig. 1F; spike number: $340 \pm 106\%$ increase, $p = 0.04$, $n = 5$).

MCS revealed an interesting trend in its effects on αRGC excitability by elevating endogenous H_2O_2. In general, αRGCs with high metabolic demand produced fewer spikes after treatment, while cells with a relatively low metabolic demand responded with heightened excitability. However, this experimental paradigm does not eliminate the possibility that the effects of MCS were exerted on the presynaptic network. In fact, since bath-applied MCS likely exerts actions on all pre-RGC neuronal circuitry and glial function, by comparing the RGC firing pattern changes and rates in Figure 1 with those in Figure 2 (see also Fig. 4), which use ROS-increasing agents that act only on the recorded RGC, these data support the conclusions that major effects can be largely attributed to intrinsic RGC mechanisms.

Somatically applied H_2O_2 or glutathione modulate sustained but not transient RGC light responses in opposite directions

To avoid presynaptic effects, a relatively low (100 μM) concentration of H_2O_2 was applied using a puffer pipette located close to the cell soma. This allowed the rapid onset of effects and limited them largely to the cell soma. In ON and OFF sustained αRGCs, H_2O_2 caused a substantial reduction in light-evoked spiking (Fig. 2A: ON sustained cells: spike rate, $23.3 \pm 11.3\%$ reduction; $p = 0.002$; spike number, $8.7 \pm 3.9\%$ reduction; $p = 0.003$, $n = 6$; Fig. 2C: OFF sustained cells: spike number, $34.5 \pm 11.0\%$ reduction; $p = 0.02$; $n = 7$). The tendency for the light response in sustained αRGCs to become more transient in MCS also occurred following H_2O_2 application. In transient αRGCs, there were no significant changes following somatic H_2O_2 (Fig. 2B: ON transient cells, 25% reduction, $n = 7$; Fig. 2D: OFF transient cells, 5% reduction, $n = 11$).

The same protocol was used to apply a membrane-permeant analog of the antioxidant GME (5 mM). GME was puffed on the cell for $\sim$30 s, then the puffer pipette was removed and light responses were recorded following 10–15 min to allow the reduction of endogenous ROS. In sustained cells, GME

increased light-evoked activity (Fig. 2A: ON sustained cells: spike number, $224 \pm 25.8\%$ increase; $p = 0.006$; $n = 9$; Fig. 2C: OFF sustained cells: spike number, $191 \pm 31.9\%$; $p = 0.01$; $n = 8$). GME applied to transient RGCs caused insignificant increases (Fig. 2B: ON transient cells, $n = 8$; Fig. 2D: OFF transient cells, $n = 8$). These results suggest that endogenous ROS act as powerful intrinsic neuromodulators in RGCs having high metabolic rates but have essentially no effect in cells with much lower metabolic demand.

Compared with bath application, this method of limiting drug application to the vicinity of the cell soma reduces effects on large numbers of upstream neurons but does not rule out modest penetration of the drugs into presynaptic networks. To isolate stimulus and response to individual αRGCs, currents step of 1 s duration were injected to drive cell spiking directly. Spontaneous activity was eliminated by frequently adjusting each RGC resting potential to be near -72 ± 3 mV using steady-state injection of hyperpolarizing current (-50 to -200 pA). We fit and quantified the nonlinear, cumulative spiking response during injected current steps with a sigmoidal curve and report the half-maximal injected current ($I_{1/2}$) and maximal spike rate of the fit. Sustained αRGCs showed significant reductions in spike number. In ON sustained cells, this was $23.4 \pm 13.2\%$ of control ($p = 0.002$, $n = 6$; Fig. 3A), and in OFF sustained cells the reduction was $43.4 \pm 8.2\%$ of control ($p = 0.02$, $n = 7$; Fig. 3C). There was no significant change to $I_{1/2}$. The application of GME produced significant increases in spike number in OFF sustained cells of $141.6 \pm 15.0\%$ ($p = 0.01$, $n = 8$; Fig. 3C). GME also caused significant leftward shifts in $I_{1/2}$ in sustained cells. ON sustained cells showed a shift of 35.4 ± 7.1 pA ($p = 0.001$, $n = 9$; Fig. 3A), while OFF sustained cells showed a shift of 24.1 ± 7.2 pA ($p = 0.004$, $n = 8$; Fig. 3C). Despite an apparent trend to follow sustained αRGCs, H_2O_2 and GME failed to significantly change parameters of the spike response to injected current steps in transient cells (Fig. 3B,D).

These results suggest that H_2O_2 dramatically modulates the excitability of sustained αRGCs but has little to no effect on transient cells. We noted that reducing endogenous ROS with a membrane-permeant analog of the endogenous antioxidant glutathione dramatically increased excitability in sustained cells, suggesting that endogenous the ROS level in sustained cells is high enough to modulate excitability in an ongoing manner. Increases in excitability occurred in sustained cells in response to both light and steps of current, suggesting that ROS modulates the intrinsic properties of sustained RGCs rather than having its actions via inputs from presynaptic networks.
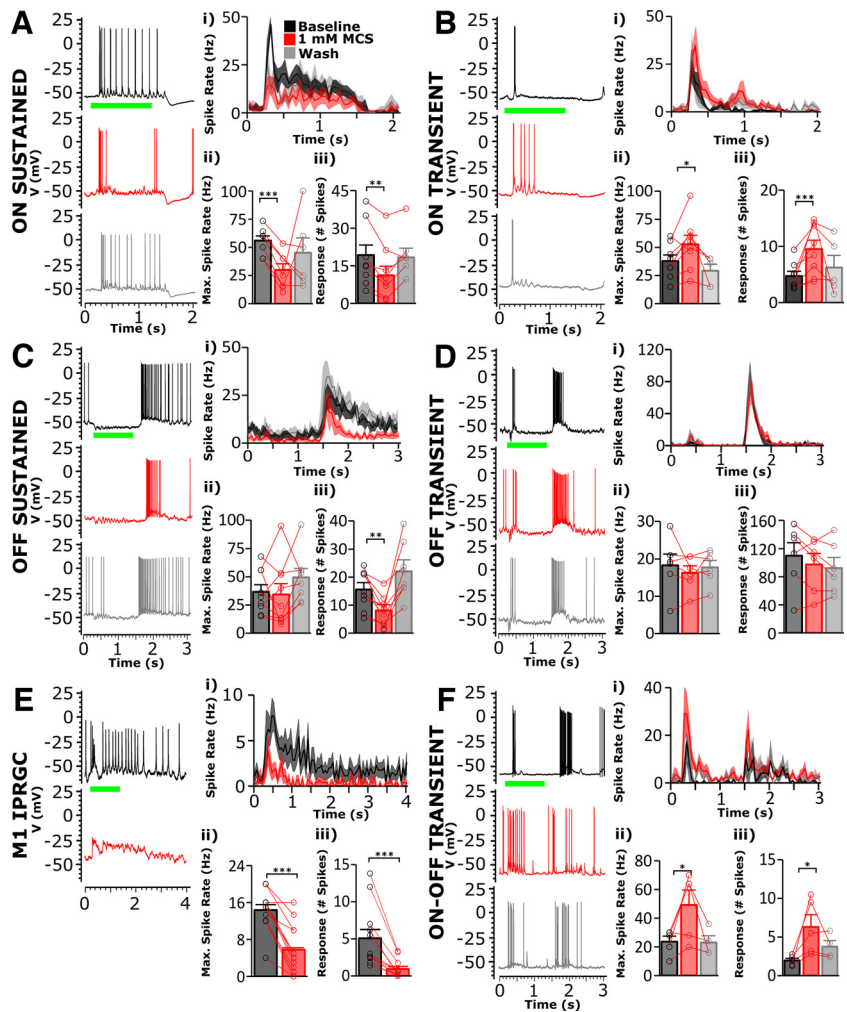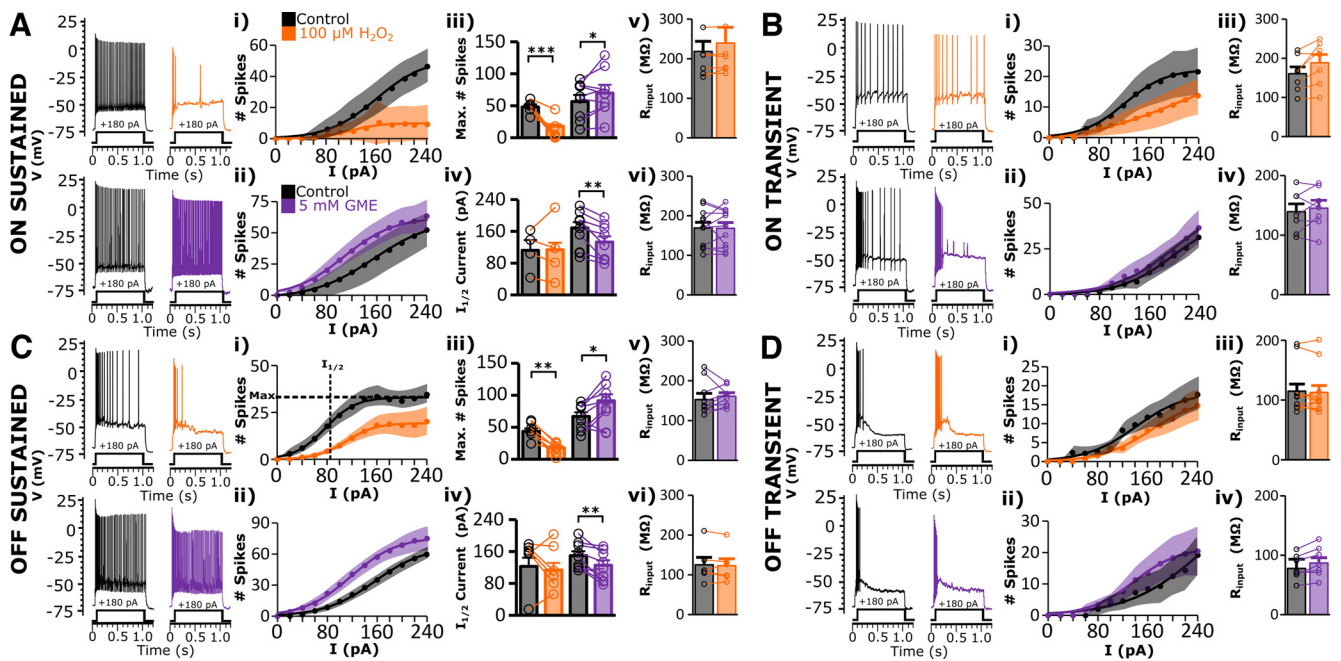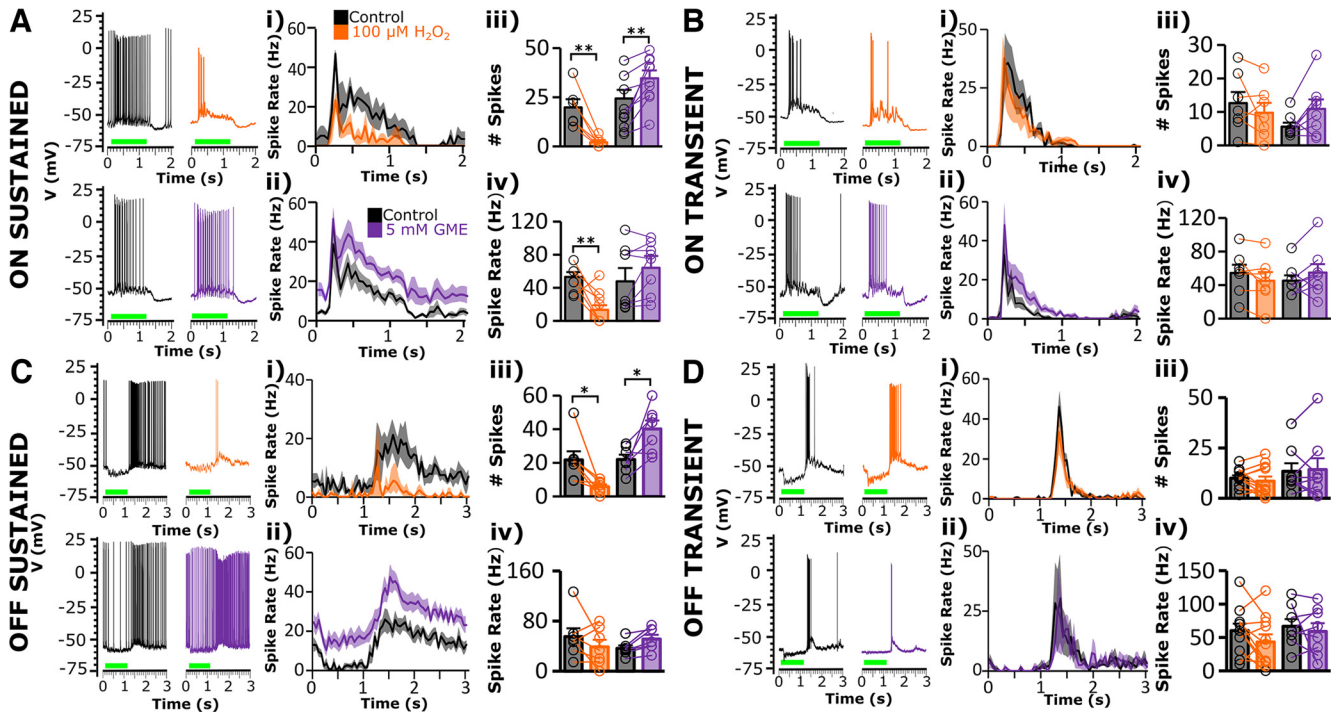

Figure 1. Increasing endogenous H_2O_2 with bath-applied MCS, which reversibly blocks glutathione peroxidase, reduces spiking in ON and OFF sustained αRGCs and M1 RGCs, and elevates spiking in ON transient αRGCs and ON-OFF RGCs, has no effect on OFF transient αRGCs. Fully reversible action of MCS (1 mM, red traces) reduced light-evoked spiking in ON sustained αRGCs (**A**) and OFF sustained (**C**) αRGCs, no effect was seen in OFF transient αRGCs (**D**), and increased spiking was seen in ON transient αRGCs (**B**) and ON-OFF transient RGCs (**F**), with irreversible reduction of spiking in M1 ipRGCs (**E**). **A–E**, In each panel set, current-clamped responses to a 1.2 s light stimulus are shown before, during (red trace), and after washout of MCS (1 mM). **Ai–Fiii**, Accompanying summary graph trios provide comparisons of the opposing MCS effects on poststimulus time histogram (**Ai, Bi, Ci, Di, Ei, Fi**), maximum spike rate (**Aii, Bii, Cii, Dii, Eii, Fii**), and cumulative spike count (**Aiii, Biii, Ciii, Diii, Eiii, Fiii**) during the light response (1.2 s). Shaded areas in traces and error bars indicate the SEM ($N = 5$–15 cells/ RGC type). Number of asterisks denotes statistical significance: *($p < 0.05$), **($p < 0.01$), ***($p < 0.001$).

Increasing mitochondrial ROS with intracellular application of the Complex III poison, antimycin-A, replicates the reduction in excitability in sustained cells

Although focal application of H_2O_2 and GME should largely limit the effects on presynaptic circuitry, the effects of altered ROS levels on the intrinsic properties of the αRGCs were further isolated by including oxidant-modulating agents in the recording pipette. We used catalase (200–500 IU/ml), a naturally present enzyme that speeds decomposition of H_2O_2 to H_2O and O_2 or antimycin-A (2 μM), which blocks Complex III (cytochrome reductase) of the electron transport chain, increasing mitochondrial superoxide. ATP was present in the internal solution, so this change cannot be attributed to reductions in energy supply. Like H_2O_2, antimycin-A caused significant reductions in light-evoked spiking in sustained αRGCs. The ON sustained cell spike rate was reduced to $63.2 \pm 11.2\%$ of control (same cell, baseline recordings following break-in; $p = 0.03$, $n = 7$), and the number of spikes was reduced to $36.3 \pm 16.9\%$ of control ($p = 0.03$, $n = 7$;
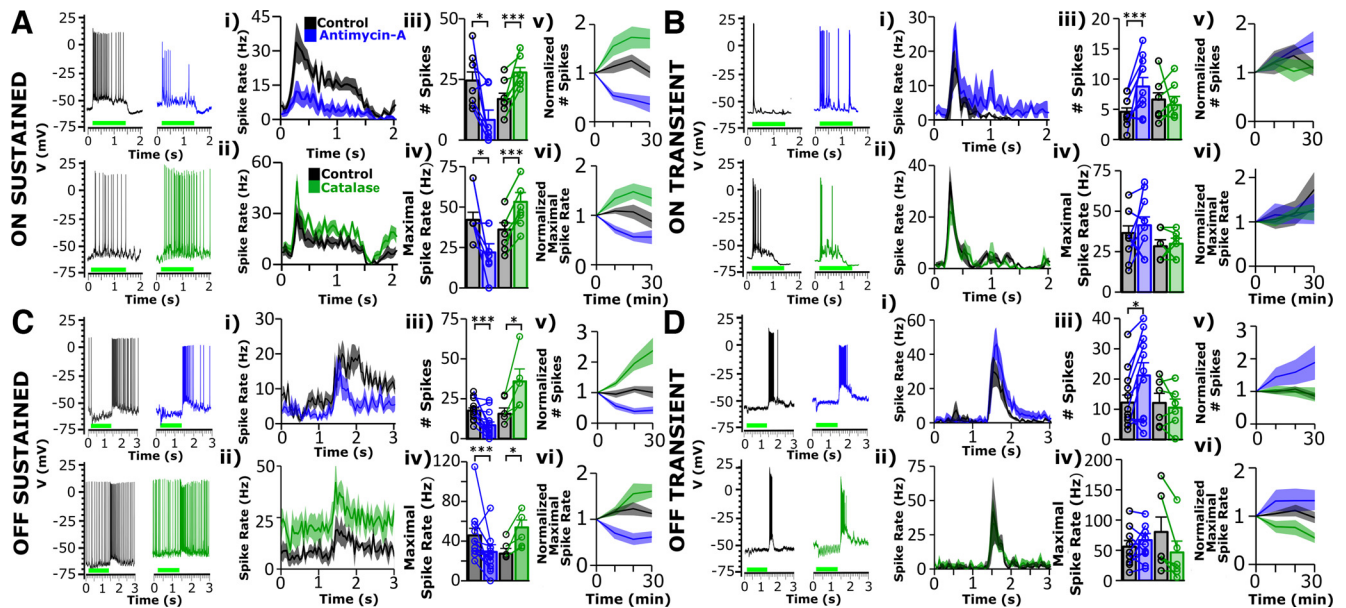
Figure 2. Focal application of membrane-permeant H_2O_2 or GME modulates light responses in opposite directions in sustained versus transient cells. **A–D**, Focal application of H_2O_2 (100 μM, orange) using a puffer pipette near the cell soma decreased light-evoked spiking in ON and OFF sustained RGCs (**A**, **C**), but had no significant effect in ON and OFF transient αRGCs (**B**, **D**). In contrast, glutathione monoester (5 mM, purple) increases light-evoked spiking in ON and OFF sustained αRGCs but has no significant effect on transient αRGCs. In each panel set, current-clamped responses to a 1 s light stimulus are shown for baseline (black), and focally applied H_2O_2 (orange) or GME (purple) via puffer pipette near the cell soma. **Ai–Dii**, Peristimulus time histograms show averaged responses for 8–12 cells in each group. **Aiii–Div**, Accompanying summary graphs allow comparison of the maximum spike rate in frequency (in Hz) and cumulative spike count during the 1 s light response. Input resistances are reported for these RGCs (Fig. 3Av,vi, Biii,iv, Cv,vi, Diii,iv). Shaded areas and error bars indicate the SEM. Number of asterisks denotes statistical significance: *($p < 0.05$), **($p < 0.01$).

Figure 3. Focal application of H_2O_2 or antioxidant GME modulates spiking in response to injected current in opposite directions in sustained but not transient αRGCs. Modulating ROS levels during responses to injected depolarizing current suggest that the effects of modulating ROS levels are predominately on intrinsic cellular properties rather than synaptic input. **A–D**, Focal application of H_2O_2 (100 μM, orange) using a puffer pipette near the αRGC soma decreased current-evoked spiking in ON and OFF sustained RGCs (**A**, **C**), but had no significant effect in ON and OFF transient αRGCs (**B**, **D**). In contrast, glutathione monoester (5 mM, purple) increases current-evoked spiking in ON and OFF sustained αRGCs but has no significant effect on transient αRGCs. In each panel set, current-clamped responses to a 1 s, 180 pA current step are shown for baseline (black), and focally applied 100 μM H_2O_2 (orange) or GME (purple) via puffer pipette near the cell soma. Cells were induced to rest near −70 mV with steady current injection to eliminate spontaneous activity. **Ai,ii, Bi,ii, Ci,ii, Di,ii**, Responses to a series of current steps (0–260 pA in 20 pA increments) are shown and fit with a sigmoid curve. **Aiii,iv, Ciii,iv**, Maximum spike number and $I_{1/2}$ were calculated and plotted. **Av,vi, Biii,iv, Cv,vi, Diii,iv**, Input resistances are reported for these cells. **B**, **D**, No significant changes in response to injected current were seen in transient cells. Shaded areas and error bars indicate the SEM. Number of asterisks denotes statistical significance: *($p < 0.05$), **($p < 0.01$), ***($p < 0.001$).

Figure 4. Intracellular application of antimycin-A (AA) and catalase produce opposite effects on light-evoked spiking. *A, C,* Pipette perfusion of AA (2 μM, blue; after 30 min), which blocks Complex III of the electron transport chain causing an increase in mitochondria-derived ROS, reduces light-induced spiking in ON and OFF sustained RGCs, while catalase (200–500 IU/ml, green) increases it. *B, D,* In ON and OFF transient RGCs, the opposite effect is seen, with increases in spiking particularly in ON transient cells with AA and no effect of catalase. In each panel set, current-clamped responses to a 1.2 s light stimulus are shown. *Ai–Dii,* Peristimulus time histograms show averaged responses for N = 5–12 cells in each group. *Aiii–Div,* Accompanying summary graphs provide comparisons of cumulative spike count during the 1 s light response and the maximum spike rate (in Hz). *Av–Dvi,* Graphs show cumulative spike rates and maximum spike rates during light responses during the 30 min perfusion of reagents normalized to time 0. Black traces were from control RGCs of the same subtype recorded for 30 min without inclusion of any drug (ON sustained, n = 5; OFF sustained, n = 5; ON transient, n = 6; OFF transient, n = 7). Input resistances are reported for these cells (Fig. 5Av,vi, Biii,iv, Cv,vi, Diii,iv). Shaded areas and error bars indicate the SEM. Delivery of AA via the patch pipette prevented reversibility. Number of asterisks denotes statistical significance: *(p < 0.05), ***(p < 0.001).

Fig. 4A). The OFF sustained cell spike rate was reduced to 61.2 ± 7.7% of control (p = 0.01, n = 14), and spike number was reduced to 43.6 ± 9.9% of control (p = 0.0005, n = 14; Fig. 4C). Changes in spike rate and number mostly occurred within 10 min after break-in and remained stable over 30 min of recording. Recordings from ON (n = 5) and OFF (n = 5) sustained cells over 30 min with control internal solution (Fig. 4Av,vi,Cv,vi, black) did not show significant run-up or rundown, indicating that these changes are unlikely to be because of bleaching or time-dependent degradation in cell condition. When catalase was included in the recording pipette, effects opposite to those of antimycin-A occurred in sustained cells and were similar to GME effects. Both ON and OFF sustained cells underwent significant increases in excitability within 10 min post break-in and were stable for 30 min. ON sustained cells showed spike rates of 134.9 ± 19.3% of control (p = 0.001) and spike numbers at 171.2 ± 20.3% of control (p = 0.007, n = 9; Fig. 4A), while OFF sustained cells showed spike rates of 138.0 ± 26.0% of control (p = 0.006) and spike numbers of 236.9 ± 42.3% of control (p = 0.03, n = 7; Fig. 4C). In transient cells, antimycin-A generally increased the number of spikes produced during light responses, with ON transient cells showing spike numbers of 164.2 ± 22.1% of control (p = 0.009, n = 8; Fig. 4B) and OFF transient cells with spike numbers of 188.5 ± 53% of control (p = 0.02, n = 11; Fig. 4D). Like GME, catalase failed to significantly alter excitability in these cells.

The effects of antimycin-A and catalase were further assessed in sustained and transient αRGCs using injected current. Here we found that antimycin-A significantly reduced maximal spike rate in sustained cells (Fig. 5A: ON sustained cells: 33.9 ± 8.9% of control; p = 0.001; n = 8; Fig. 5C: OFF sustained cells: 75.6 ± 10% of control; p = 0.0007, n = 13) but not in $I_{1/2}$. After 30 min of catalase,

there were significant increases in maximal spike rate in sustained cells (Fig. 5A: ON cells: 124.4 ± 11.7% of control; p = 0.047; n = 7; Fig. 5C: OFF cells: 145.7 ± 14.9% of control; p = 0.02; n = 5). Catalase did not change the $I_{1/2}$ significantly in sustained cells. Whereas there was generally an increase in the number of light-evoked spikes in transient cells (Fig. 4), there was no significant change in current-evoked spiking (Fig. 4), and this effect did not stabilize within 30 min. No significant change in transient cells with catalase was observed (Fig. 5B,D), suggesting that at baseline there is little to no modulation of transient cells by a standing level of ROS.

Biophysical mechanisms underlying the modulation of action potential efficiency and frequency by ROS-mediated feedback in RGCs

Given the changes in response to injected current in sustained cells we hypothesized that increased spiking activity of αRGCs drives elevations in intracellular ROS levels and that these elevated ROS levels modulate the gating of the ion channels underlying action potential generation. To assess how ROS affect the Na_V channels that underlie the intrinsic excitability of each αRGC type and to assess biophysical differences between sustained and transient αRGCs, changes in the shape of action potentials in sustained versus transient cells following localized puff application of 100 μM H_2O_2 were determined. At baseline, transient cells produced relatively few spontaneous action potentials, so we injected Gaussian white noise current (μ = 0 pA², σ = 16 pA², 50 Hz sampling rate; MATLAB random number generator) to modestly increase spike generation (Fig. 6A–D). Somatically applied 100 μM H_2O_2 caused significant reductions in action potential height in all cell types (ON sustained: $p < 1 \times 10^{-10}$, n = 4 cells; OFF sustained: $p < 1 \times 10^{-10}$, n = 8 cells; OFF transient: $p < 1 \times 10^{-10}$, n = 5 cells; ON transient:
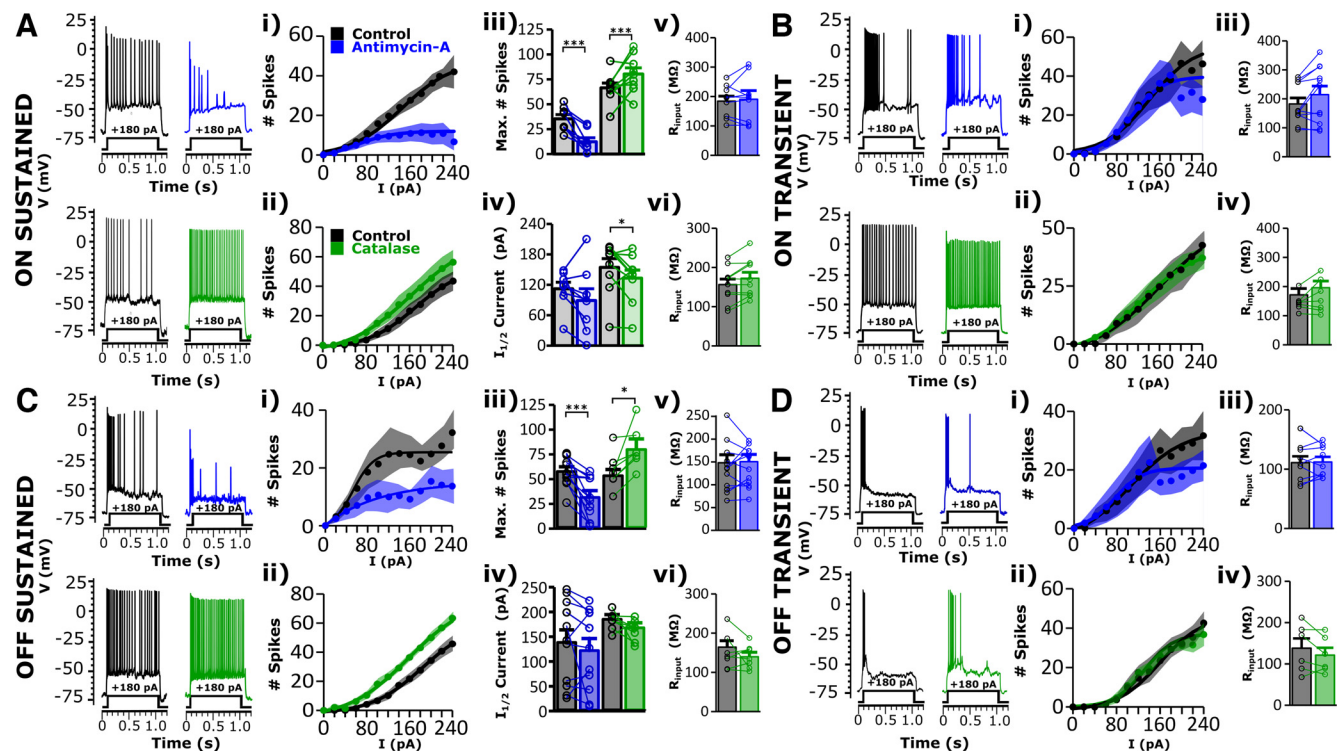
Figure 5. Intracellularly applied antimycin-A (AA) and catalase produce opposite effects on spiking in response to current injection in sustained cells but not in transient cells. Modulating ROS levels during responses to injected current suggest that the effects of modulating ROS are predominately on intrinsic cellular properties rather than synaptic input. **A–D**, Intracellular delivery of AA (2 μM, after 30 min) decreased current-evoked spiking in ON and OFF sustained αRGCs (**A, C**), but had no significant effect on ON or OFF transient αRGCs (**B, D**). In contrast, intracellular delivery of catalase (200–500 IU/ml, green) increased current-evoked spiking in ON and OFF sustained αRGCs, but there was no significant effect on transient αRGCs. In each panel set, current-clamped responses to a 1 s, 180 pA current step are shown for baseline (black), after 30 min of AA either (blue) or catalase (green). Cells were induced to rest near −70 mV with steady current injection to eliminate spontaneous activity. **Ai–Dii**, Responses to a series of current steps (0–260 pA in 20 pA increments) are shown and fit with a sigmoid curve. **Aiii,iv, Ciii,iv**, Maximum spike number and $I_{1/2}$ were calculated and plotted. **B, D**, No significant changes in response to injected current were seen in transient cells. **Av,vi, Biii,iv, Cv,vi, Diii,iv**, Input resistances are reported for these cells. Shaded areas and error bars indicate the SEM. Number of asterisks denotes statistical significance: *($p < 0.05$), ***($p < 0.001$).

$p = 0.0001$, $n = 4$ cells; Mann–Whitney U test) and increases in half-width in all except ON transient cells (ON sustained, $p < 1 \times 10^{-10}$; OFF sustained, $p < 1 \times 10^{-10}$; OFF transient, $p = 0.01$). However, the effect in sustained cells was much larger in all cases. H_2O_2 reduced spike amplitude in ON transient cells by ~5% versus ~45% in ON sustained cells, and half-width increased by ~250 μs versus ~1.7 ms in the same cells. In OFF cells, the same general pattern emerged with ~5% reduction in spike height in OFF transient cells versus ~25% in ON sustained cells and a 250 versus 350 μs increase in half-width. The slope of the membrane voltage during the action potential (dV/dt) was calculated as an approximation of Na$_V$ channel availability (Colbert et al., 1997; Weick and Demb, 2011). H_2O_2 caused a significant reduction in dV/dt in all cell types (ON sustained, $p < 1 \times 10^{-10}$; OFF sustained, $p < 1 \times 10^{-10}$; OFF transient, $p < 1 \times 10^{-10}$; ON transient cells $p = 5.7 \times 10^{-9}$); however, in sustained cells the reduction was much larger than in transient RGCs (Fig. 6A,C: ON cells: dV/dt ~65% of control in sustained vs 85% of control in transient; Fig. 6B,D: OFF cells: ~60% of control in sustained vs 95% of control in transient).

Observing the properties of action potentials suggested that the reduction in spiking in sustained αRGCs might be because of reductions in Na$_V$ current. To test this mechanism more explicitly, the nucleated patch technique was used to assess the effects of H_2O_2 on whole-cell Na$_V$ current in identified αRGCs. We identified αRGCs by extracellular light response (Fig. 7B–E), and then, following nucleation, 100 μM H_2O_2 was puff applied from a nearby pipette (Fig. 7A).

In nucleated patch recordings, inward currents could be completely blocked by 1 μM TTX (Fig. 7Ai,ii). The 100 μM H_2O_2 significantly reduced peak current in sustained but not transient αRGCs (Fig. 7F,G: sustained cells: 68.9 ± 2.7% of control; $n = 15$; $p = 0.0002$; transient cells: 106.1 ± 3.4% of control; $n = 14$). The inactivation curves for nucleated patches from αRGCs were left shifted with a mean inactivation half-maximal voltage ($V_{1/2}$) of −102.4 ± 5.3 mV. Nucleated patch recordings from other RGC types (e.g., M1 RGCs) did not present with this shifted inactivation $V_{1/2}$ (−66.7 ± 1.3 mV), suggesting that this was not a limitation of the technique itself but was caused by some other feature of αRGCs, possibly their unusually large somata. This limited our ability to assess the voltage dependence of inactivation as a possible mechanism underlying the reduced current following H_2O_2 (Fig. 7I). However, there were significant leftward shifts in activation in both sustained and transient cells (Fig. 7H; sustained cells: −3.5 ± 0.9 mV; $p = 0.0017$; transient cells: −3.6 ± 1.4 mV; $p = 0.02$).

We noted that elevating ROS typically made the spiking response to either current injection or light to become more transient in sustained αRGCs and the nucleated patch recordings implicated reduction of Na$_V$ current as a plausible mechanism. This is similar to studies of Na$_V$1.1 knock-out mice, which show a similar deficit in repetitive spiking (Yu et al., 2006; Ogiwara et al., 2007). In OFF transient αRGCs, a similar increase in transience was observed in response to injected current using 500 nM 4,9-anhydrotetrodotoxin (4,9ahTTX; Werginz et al., 2020). At this concentration, 4,9ahTTX blocks both Na$_V$1.1 and Na$_V$1.6 (Griffith et al., 2019; Denomme et al., 2020; Werginz et al., 2020).
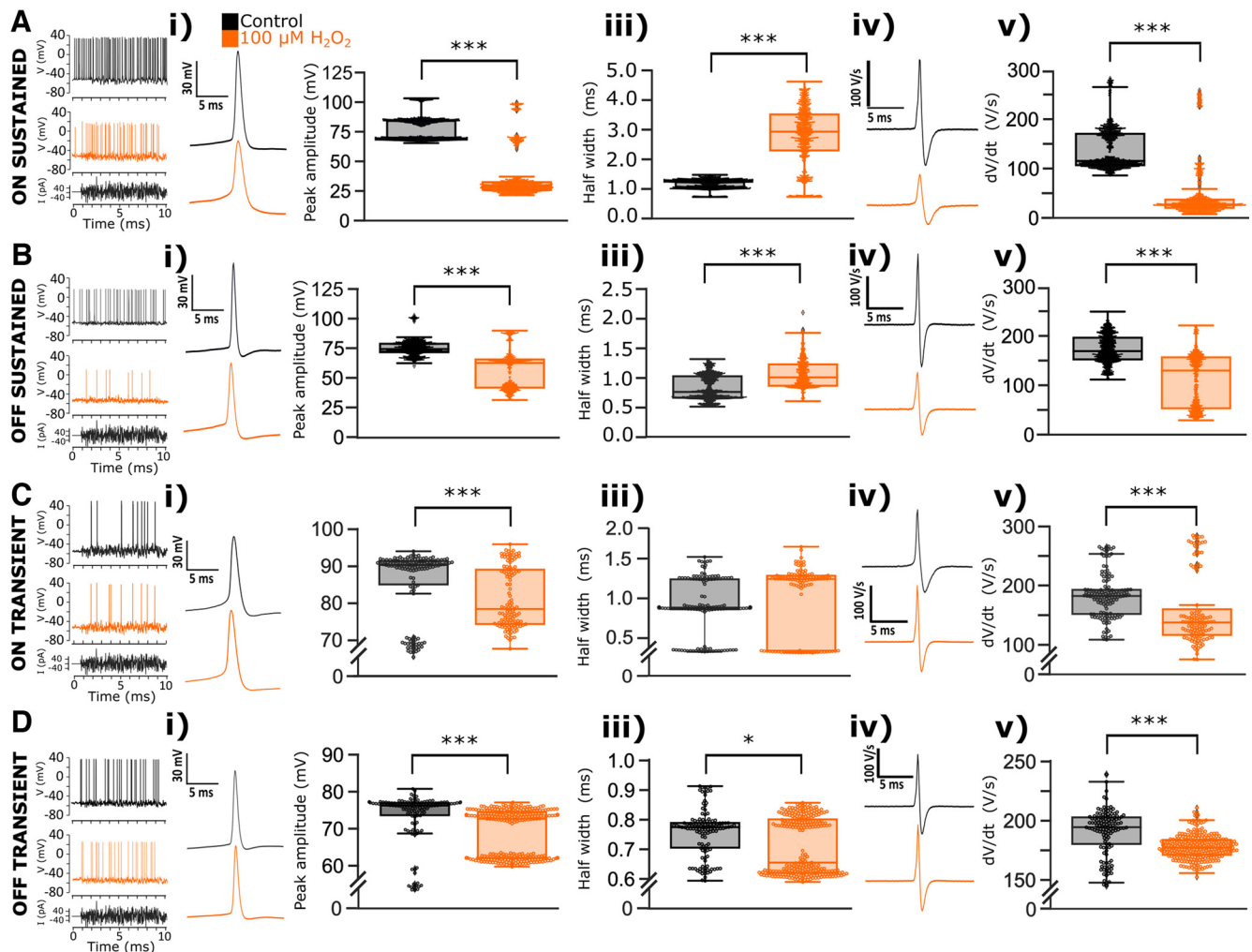
Figure 6. Localized application of H_2O_2 causes larger changes in single spike parameters in sustained αRGCs than in transient αRGCs. *A–D*, Gaussian white noise current injection was used to evoke spikes from αRGCs (*A*, ON sustained; *B*, OFF sustained; *C*, ON transient; *D*, OFF transient) under control (black traces) and following somatically applied 100 μM H_2O_2 (orange traces). *Ai*, *Bi*, *Ci*, *Di*, Exemplar single spikes are shown. *Aii–Diii*, Quantification of spike peak amplitude (*Aii*, *Bii*, *Cii*, *Dii*) and half-width (*Aiii*, *Biii*, *Ciii*, *Diii*) show significant reductions in spike height and increases in half-width in all cells, but with much larger disparities in ON and OFF sustained cells. *Aiv*, *Biv*, *Civ*, *Div*, dV/dt values are shown before and after 100 μM H_2O_2. *Av*, *Bv*, *Cv*, *Dv*, Quantification of dV/dt changes before and after H_2O_2. Box and whisker plots show interquartile range and mean [ON transient (ON-T), $n = 4$ cells; OFF-T, $n = 5$ cells; OFF saturation (OFF-S), $n = 8$ cells; ON-S, $n = 3$ cells]. Input resistances are reported for these RGCs (Fig. 3*Av,vi,Biii,iv,Cv,vi,Diii,iv*). Number of asterisks denotes statistical significance: *($p < 0.05$), ***($p < 0.001$).

However, a highly specific $Na_V1.1/1.3$ channel blocker, ICA121431 (Griffith et al., 2019), is selective for $Na_V1.1$ and 1.3 over the $Na_V1.2$ and $Na_V1.6$ channel isoforms also expressed by RGCs (Van Hook et al., 2019). Although ICA121431 is nonselective between $Na_V1.1$ and $Na_V1.3$, $Na_V1.3$ is normally expressed primarily in the developing, nonadult nervous system (Waxman et al., 1994; Felts et al., 1997) and is also upregulated after injury (Waxman et al., 1994; Gastaldi et al., 1997). Because of these constraints, we consider the most likely Na_V channel isoform blocked by ICA121431 in this current study to be $Na_V1.1$, notwithstanding earlier detection of $Na_V1.3$ mRNA in RGC somata using *in situ* hybridization (Fjell et al., 1997). Regardless of the isoform responsible, blocking $Na_V1.1/1.3$ channels replicates the selective effects of ROS elevation on sustained cells and prevents additional ROS effects.

Somatic application of ICA121431 (500 nM) was used to first assess whether blocking $Na_V1.1/1.3$ channels might have different effects on sustained and transient αRGCs (Fig. 8). ICA121431 caused the light response of sustained αRGCs to become much more transient, mimicking the effect of H_2O_2, antimycin-A, and MCS (Fig. 8*A*: ON sustained cells: spike number, $38.3 \pm 5.1\%$ of

control; $p = 0.0002$; $n = 6$; Fig. 8*C*: OFF sustained cells: spike number, $31.5 \pm 6.3\%$ of control; $p = 0.01$; $n = 9$). Maximal spike rate tended to be reduced, but this was not significant. In transient αRGCs, the effect of ICA121431 was much less pronounced, and, although a mean reduction in the number of spikes was seen in OFF transient αRGCs ($n = 5$), this did not reach significance (Fig. 8*B,D*). Following the application of ICA121431, the puffer pipette was replaced with one containing both ICA121431 and 100 μM H_2O_2. When $Na_V1.1/1.3$ was blocked with ICA121431, there was little additional effect of H_2O_2 in either sustained or transient αRGCs. The one exception was that, whereas ICA121431 alone did not significantly reduce maximal spike rate in ON sustained αRGCs, the combination of ICA121431 plus H_2O_2 did ($p = 0.01$; one-way ANOVA with *post hoc* Tukey's HSD test). The treatments with ICA121431 and ICA121431 plus H_2O_2 are not significantly different from each other ($p = 0.68$).

The effects of ICA121431 alone and in combination with H_2O_2 on the response to injected current was also tested. ICA121431 caused a significant reduction in maximal spike rate in sustained αRGCs (Fig. 9*A*: ON sustained cells: spike rate, $60.0 \pm 10.4\%$ of control; $p = 0.04$; $n = 6$; Fig. 9*C*: OFF sustained cells: spike number,
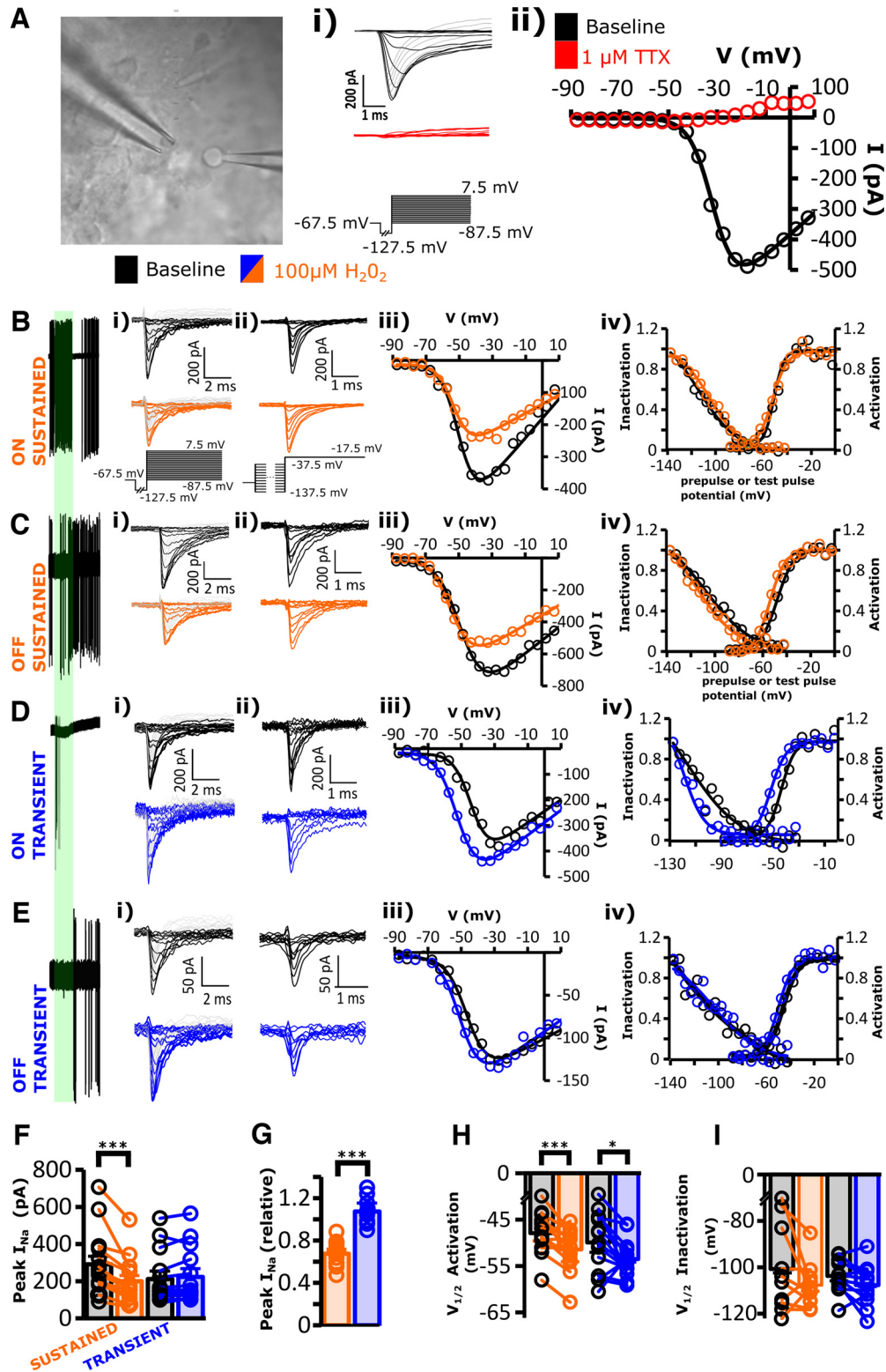
Figure 7. Peak Na$_V$ current is reduced by H$_2$O$_2$ in nucleated patches from sustained but not transient αRGCs. *A*, Puff pipette loaded with 100 μM H$_2$O$_2$ is positioned close to the nucleated patch following removal from an identified αRGC. *Ai*, Depolarizing voltage steps in a nucleated patch before and after a 1 μM TTX puff (red traces) to demonstrate selective efficacy for Na$_V$ channel block. *Aii*, Na$_V$ channel current–voltage relationship. *B–E*, Leftmost columns show identification of αRGCs by extracellular ("loose patch") light responses (1 s light stimulus, green bar) before rupture. *Bi,ii, Ci,ii, Di,ii, Ei,ii*, Na$_V$ currents in response to depolarizing voltage steps (*Bi, Ci, Di, Eii*) and 200 ms inactivating prepulse steps (*Bii, Cii, Dii, Eii*) in control and H$_2$O$_2$ (100 μM; sustained cells, orange traces; transient cells, blue traces). *Bi,iv, Ci,iv, Di,iv, Ei,iv*, Na$_V$ channel current–voltage relationship from example cells (*Bi, Ci, Di, Ei*), and their activation and inactivation curves (*Biv, Civ, Div, Eiv*). *F*, Significant peak current reductions were seen in sustained αRGCs ($n = 14$) but not in transient αRGCs ($n = 13$). *G*, Normalized peak currents show significant differences in the percentage of change following H$_2$O$_2$ in sustained but not transient αRGCs. *H*, Significant negative shifts of $V_{1/2}$ of activation occurred in both sustained and transient RGCs. *I*, Nucleated patches from αRGCs had unusually negative $V_{1/2}$ inactivation precluding meaningful analysis in inactivation kinetics. Number of asterisks denotes statistical significance: *($p < 0.05$), ***($p < 0.001$).

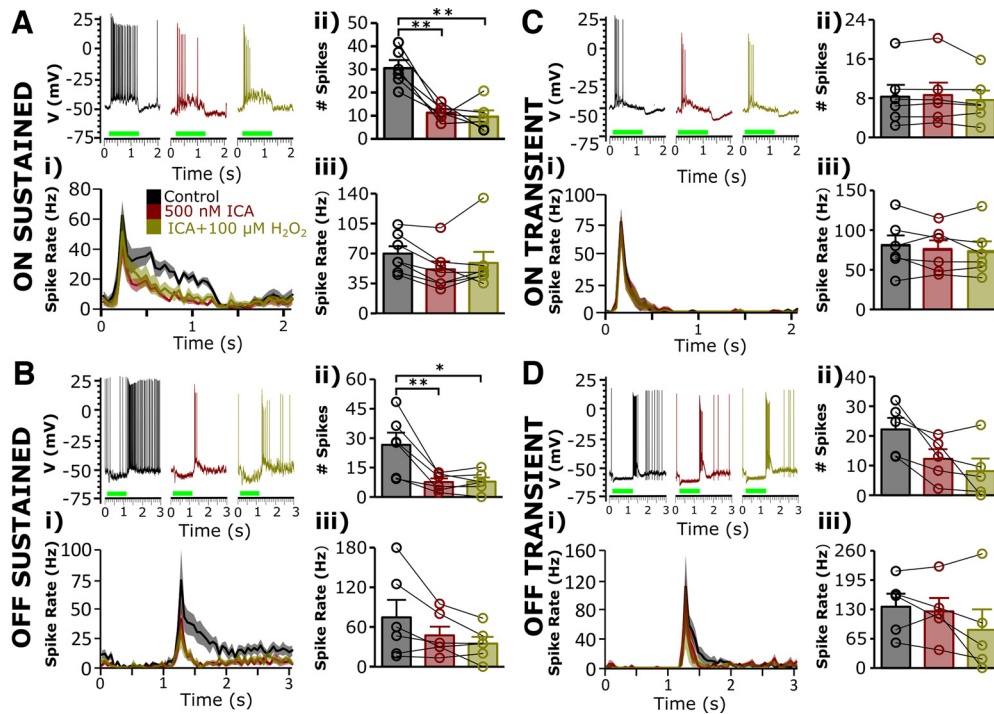**Figure 8.** Selective $Na_V1.1/1.3$ blocker ICA121431 reproduces the effect of H_2O_2 on light-evoked spiking in sustained αRGCs, and together they have little added effect. ***A–D***, Focal application of ICA121431 (500 nM; burgundy traces) using a puffer decreased spiking in ON and OFF sustained αRGCs (***A, B***) with less effect in ON and OFF transient αRGCs (***C, D***). A mix of 100 μM H_2O_2 and ICA121431 (500 nM, gold traces) had little further effect compared with ICA121431 alone. ***Ai, Bi, Ci, Di***, Peristimulus time histograms show average responses for N = 5–10 cells in each group. ***Aii, Bii***, Spike counts during the light response were significantly reduced compared with control with ICA121431 or a mix of ICA121431 + H_2O_2 in ON and OFF sustained (***Aii, Bii***) but not ON or OFF transient or αRGCs (***Cii, Dii***). ***Aiii, Biii, Ciii, Diii***, Maximum spike rate was not significantly changed in either sustained or transient αRGCs. Input resistances are reported for these cells (Fig. 9*Aii, Bii, Cii, Dii*). Shaded areas and error bars indicate the SEM. Number of asterisks denotes statistical significance: *($p < 0.05$), **($p < 0.01$).

49.7 ± 12.4% of control; $p = 0.002$; $n = 5$). Similar to the light response, the response to injected current became much more transient following treatment with ICA121431. When H_2O_2 was combined with ICA121431, we did not note any further reduction in spike rate, and in fact, there was a slight but insignificant increase in maximal spike rate. $I_{1/2}$ was not changed in sustained αRGCs in either treatment, and significant changes to the response to injected current in ON and OFF transient αRGCs in response to either treatment were not observed (Fig. 9*B,D*).

Changes to the shape of action potentials driven by either 500 nM ICA121431 alone or in combination with 100 μM H_2O_2 were also investigated. In earlier experiments, as per Figure 6, the slope of the membrane voltage during the action potential (dV/dt) was most indicative of changes in Na_V channel availability, so we focused specifically on this metric comparing the actions of ICA121431 alone or in combination with H_2O_2 on spiking in Figure 10. We found that dV/dt was significantly reduced by ICA121431 in both types of sustained αRGCs (ON sustained cells: ~60% of control; $p < 1 \times 10^{-10}$; OFF sustained cells: ~65% of control; $p < 1 \times 10^{-10}$; Kruskal–
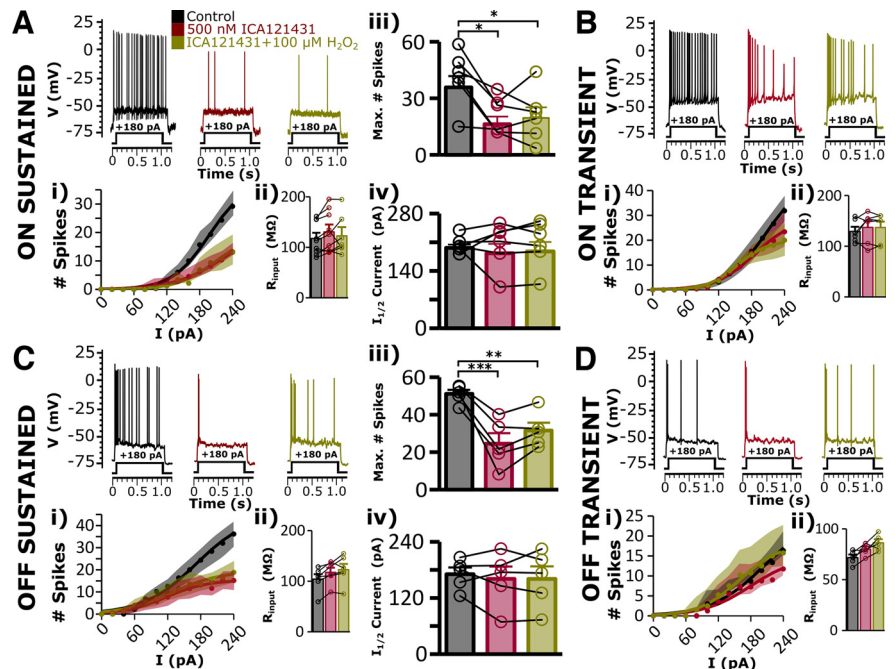

Figure 9. Selective $Na_V1.1/1.3$ blocker ICA121431 reproduces the effect of H_2O_2 on injected current-evoked spiking in sustained αRGCs, further addition of 100 μM H_2O_2 had little additional effect. ***A–D***, Focal application of ICA121431 (500 nM; burgundy) using a puffer decreased current-evoked spiking in ON and OFF sustained αRGCs (***A, C***) with no significant effect in ON and OFF transient αRGCs (***B, D***). A mix of 100 μM H_2O_2 and ICA121431 (gold) had little further effect compared with ICA121431 alone. In each panel set, current-clamped responses to a 1 s 180 pA current step are shown for baseline (black), and focal application of 500 nM ICA121431 (burgundy) or 500 nM ICA121431 + 100 μM H_2O_2 (gold). Cells were induced to rest near −72 mV with steady current injection to eliminate spontaneous activity. ***Ai, Bi, Ci, Di***, Responses to a series of current steps (0–260 pA in 20 pA increments) are shown and fit with a sigmoid curve. ***Aii, Bii, Cii, Dii***, No significant change was noted in input resistance during these experiments. ***Aiii,iv, Ciii,iv***, Maximum spike count and $I_{1/2}$ were calculated and plotted. Shaded areas and error bars indicate the SEM. Number of asterisks denotes statistical significance: *($p < 0.05$), **($p < 0.01$), ***($p < 0.001$).
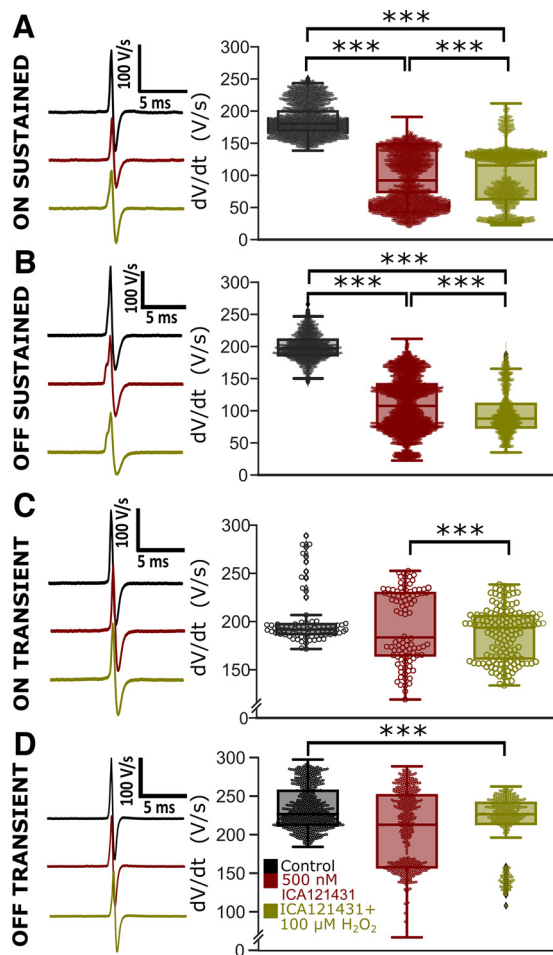
Figure 10. Selective Na$_V$1.1/1.3 blocker ICA121431 reproduces the effect of H$_2$O$_2$ on the dV/dt in sustained αRGCs. **A–D**, Gaussian white noise current injection was used to evoke spikes from αRGCs, which were then differentiated (**A**, ON sustained; **B**, OFF sustained; **C**, ON transient; **D**, OFF transient) under control (black), somatically applied ICA121431 (500 nm, burgundy), and somatically applied ICA121431 + 100 μM H$_2$O$_2$ (gold). Box and whisker plots show the quantification of dV/dt before and after ICA121431 and ICA121431 + H$_2$O$_2$. Plots show the interquartile range and mean. Number of asterisks denotes statistical significance: ***($p < 0.001$).

Wallis test with *post hoc* Dunn's test for multiple comparisons) and further treatment of 100 μM H$_2$O$_2$ + 500 nM ICA121431 caused a small additional decrease in both cell types (ON sustained cells, ~55% of control: $p < 1 \times 10^{-10}$ vs control and ICA121431 alone; OFF sustained cells, 50% of control: $p < 1 \times 10^{-10}$ vs control and ICA121431 alone). In contrast to sustained αRGCs, relatively small reductions in transient αRGCs were noted (ON transient cells: ICA121431, ~90% of control; ICA121431 + H$_2$O$_2$, ~90% of control; $p = 0.63$ vs control; $p = 0.005$ vs ICA121431 alone; OFF transient cells: ICA121431, 95% of control, $p = 0.46$; ICA121431+ H$_2$O$_2$, ~90% of control, $p = 0.0024$). These results demonstrate that the majority of the effects observed with H$_2$O$_2$, and presumably with other ROS-elevating treatments, can be replicated by blocking Na$_V$1.1/1.3 in sustained αRGCs.

Discussion

Neurons have highly diverse electrogenic phenotypes. Understanding why some biophysical phenotypes are favored is a key step in deepening our understanding of what neurons are optimized for in diverse neural tissues. Minimizing energetic cost is emerging as a powerful evolutionary constraint on successful neural phenotypes. We investigated whether ROS, produced as an inevitable consequence of ATP production, might act intrinsically to modulate the excitability of sustained RGCs having high metabolic demand. A wide variety of ROS-manipulating reagents revealed that in sustained but not transient RGCs, ROS elevation reduced excitability. Reducing ROS by augmenting the natural antioxidant abilities of the cells increased excitability in sustained RGCs with no effect on transient RGCs. The expression of Na$_V$1.1/1.3 channels, found to be necessary for sustained αRGCs to produce tonic spiking in response to prolonged light, also endows these cells with a feedback mechanism that limits spike rate. This connection between electrogenic phenotype and energy-conserving adaptation is broadly consistent with metabolically efficient coding, although further work is necessary to test the relationship between information bandwidth and energetic demand with and without Na$_V$1.1/1.3 function.

Sustained, but not transient, αRGCs have tonically elevated ROS levels that intrinsically modulate excitability

Neurons are constantly producing ROS and superoxide as a consequence of ATP production. Tonically elevated ROS is known to cause neurodegeneration, so neurons typically use antioxidants (e.g., catalase, glutathione peroxidase, superoxide dismutase, vitamins C and E) to control ROS levels. Here we provide evidence that ROS levels act as neuromodulators. Augmenting the natural antioxidant capacity of RGCs with catalase or GME increased excitability dramatically in sustained, but not transient, αRGCs. Both light-evoked and current-evoked spiking increased in sustained αRGCs following ROS reduction, suggesting that the mechanism of action was on cellular intrinsic properties rather than synaptic input. This implies that tonically elevated ROS levels act as a feedback mechanism in sustained αRGCs to reduce excitability, and that excitability in these cells can be manipulated by altering the production of antioxidants.

In contrast, transient αRGCs were essentially unaffected by reducing standing ROS levels. This suggests that either ROS levels are low enough under normal circumstances that further reduction is inconsequential or the mechanism of action leading to ROS-dependent reductions is lacking in transient αRGCs. To test how ROS affect RGC function, ROS levels were modulated with three different approaches. The results of ROS elevation were consistent in sustained αRGCs. MCS, antimycin-A, and somatically applied H$_2$O$_2$ reduced excitability in response to light and injected currents, making responses more transient. The similarity between sustained αRGCs following ROS elevation and transient αRGCs under control conditions suggested that ROS might act on the intrinsic properties that allow sustained RGCs to produce tonic spiking in response to light and current injection. The effects on transient αRGCs were more dependent on the mechanism used to elevate ROS and ranged from no effect to increased excitability in response to light, with little or no effect on injected current.

ROS reduce excitability in sustained αRGCs by reducing Na$_V$1.1/1.3 channel currents

The results implicate Na$_V$ channels in having a principal role in the mechanism of action by which ROS mediate reductions in excitability in sustained αRGCs. First, it was found that the height, half-width, and temporal derivative (i.e., dV/dt) of the action potentials were strongly altered in sustained cells, but not in transient αRGCs. In particular, the slope of the rising phase of the action potential is established as a solid approximation of Na$_V$ current availability in neurons (Colbert et al., 1997; Weick

and Demb, 2011). Compared with transient αRGCs, dV/dt was greatly reduced by somatic application of H_2O_2 in sustained cells. We isolated nucleated patches from αRGCs identified by their extracellular light responses and found significant reductions in peak Na_V current following H_2O_2 in sustained but not transient cells. Surprisingly, in αRGCs, but not in other RGC types from which nucleated patches were pulled, the inactivation $V_{1/2}$ was very left shifted, and a hyperpolarizing prepulse close to $-120\,mV$ was required for full Na_V current activation, precluding meaningful analysis of the underlying voltage-dependent gating kinetics.

Our observations suggest that Na_V channels play a significant role in RGC modulation by ROS. RGCs express Na_V1.1, 1.2, 1.6, 1.8, and perhaps 1.3 (Fjell et al., 1997; Boiko et al., 2003; Van Wart and Matthews, 2006; Mojumder et al., 2007; O'Brien et al., 2008; Smith et al., 2017). While both Na_V1.1 and 1.6 have been implicated in sustained repetitive spiking, ICA121431, a blocker of Na_V1.1 (and Na_V1.3) is highly selective, while the common blocker of Na_V1.6 (4,9 anhydro-tetrodotoxin) is not selective between Na_V1.1 and 1.6 (Griffith et al., 2019; Denomme et al., 2020). When Na_V1.1/1.3 channels in sustained αRGCs were blocked with somatic application of ICA121431, their light responses were rendered more transient, similar to the effects of ROS elevation. Further application of a mix of ICA121431 and 100 μM H_2O_2 in sustained αRGCs had only minor additive effects on light-evoked and current-evoked spiking, suggesting actions on the same target. This possibility is supported as neither ICA121431 alone or in combination with H_2O_2 caused significant reductions in transient cells. When the effects of ICA121431 alone and in combination with H_2O_2 on dV/dt were assessed, we found that in sustained cells, almost the entire effect of H_2O_2 on dV/dt could be eliminated following treatment with ICA121431.

The results with the selective blocker ICA121431 are consistent with robust Na_V1.1/1.3 channel function in sustained αRGCs, not transient αRGCs. This would facilitate the high-frequency repetitive spiking and high spontaneous activity observed in these cells and create a built-in adaptive mechanism reducing firing rate when ROS levels rise and increasing excitability when ROS levels fall. These results imply that transient cells are much less affected by ROS because of their having fewer redox-sensitive Na_V channel isoforms. Previous reports provide evidence of redox modulation of Na_V channels (Evans and Bielefeldt, 2000; Fukuda et al., 2005; Kassmann et al., 2008) and differences in oxidative modulation between molecular isoforms (Kassmann et al., 2008; Schlüter and Leffler, 2016).

Transient RGCs increase in excitability following ROS elevation

Mitochondrial dysfunction drives optic neuropathies because of genetic mutations (e.g., Leber hereditary optic neuropathy, Leigh disease, dominant optic atrophy) and environmental toxins (Pilz et al., 2017). In most cases, including glaucoma, ROS accumulation is a key feature of neurodegeneration (Tezel, 2006). In optic nerve crush or transection models, where RGC ROS levels are elevated (Kanamori et al., 2010; Sayır et al., 2013; Fan et al., 2017), transient cells degenerate more rapidly (Della Santina et al., 2013; Tran et al., 2019). Our results using the Complex III toxin antimycin-A or MCS, which increase ROS, showed increased excitability in both ON and OFF transient αRGCs over 30 min. Unlike the actions of antimycin-A in sustained cells that essentially stabilized after 10 min, in transient cells the effects of antimycin-A were slower in onset and did not stabilize during the 30 min of recording time.

The mechanisms underlying changes in transient αRGC excitability bear further investigation given their relevance to chronically elevated ROS levels in disease states. It is known that H_2O_2 diffuses through membranes and can act presynaptically, increasing glutamate release in ventral dorsal horn neurons (Ohashi et al., 2016a). Our direct application of H_2O_2 to RGC somata produced no significant effect in transient αRGCs, nor did antimycin-A produce significant changes to responses to injected current, suggesting that the changes involved upstream or synaptic inputs. Earlier studies in isolated RGCs (Aizenman et al., 1989) showed that NMDA receptors were potentiated under reducing conditions and that there was no effect on AMPA/kainate receptors, suggesting that a direct action of ROS-potentiating glutamate receptors in transient RGCs was unlikely.

Inhibitory GABA and glycine synaptic currents in RGCs are decreased by oxidants and potentiated by antioxidants (Pan et al., 1995). In contrast, ROS increase some GABAergic currents (Accardi et al., 2014; Penna et al., 2014; Ohashi et al., 2016a, b). This suggests additional mechanisms by which ROS might both inhibit and excite αRGCs during chronically elevated ROS levels leading to pathologic hyperexcitability.

Our findings suggest that, compared with sustained αRGCs, transient αRGCs have much lower levels of Na_V1.1/1.3 expression (judged by their minor ICA121431 block) and that while this contributes to their reduced basal metabolic demand, it is consistent with the lack of the pronounced ROS-mediated inhibitory feedback mechanism shown here in sustained αRGCs. During antimycin-A-induced ROS increases, transient RGCs became more excitable. It will be important to pinpoint the exact mechanism underlying this increased excitability and determine its role in neurodegenerative states.

In conclusion, these results provide compelling evidence that endogenous ROS act as modulators in sustained, not transient, αRGCs, and that the mechanisms underlying this action are mediated by the intrinsic properties of the RGCs rather than arising from presynaptic mechanisms. Although substantial literature indicates that ROS modify the excitability of neurons, these novel findings specifically link intrinsic metabolic demand to a significant neuromodulatory role for ROS within neurons, here RGCs, in which the cell subtypes have widely varying basal metabolic rates and intrinsic biophysical properties.

References

Accardi MV, Daniels BA, Brown PMGE, Fritschy J-M, Tyagarajan SK, Bowie D (2014) Mitochondrial reactive oxygen species regulate the strength of inhibitory GABA-mediated synaptic transmission. Nat Commun 5:3168.

Aizenman E, Lipton SA, Loring RH (1989) Selective modulation of NMDA responses by reduction and oxidation. Neuron 2:1257–1263.

Avshalumov MV, Chen BT, Koós T, Tepper JM, Rice ME (2005) Endogenous hydrogen peroxide regulates the excitability of midbrain dopamine neurons via ATP-sensitive potassium channels. J Neurosci 25:4222–4231.

Boiko T, Van Wart A, Caldwell JH, Levinson SR, Trimmer JS, Matthews G (2003) Functional specialization of the axon initial segment by isoform-specific sodium channel targeting. J Neurosci 23:2306–2313.

Carter BC, Bean BP (2009) Sodium entry during action potentials of mammalian neurons: incomplete inactivation and reduced metabolic efficiency in fast-spiking neurons. Neuron 64:898–909.

Chuang H, Lin S (2009) Oxidative challenges sensitize the capsaicin receptor by covalent cysteine modification. Proc Natl Acad Sci U S A 106:20097–20102.

Colbert CM, Magee JC, Hoffman DA, Johnston D (1997) Slow recovery from inactivation of Na$^+$ channels underlies the activity-dependent attenuation of dendritic action potentials in hippocampal CA1 pyramidal neurons. J Neurosci 17:6512–6521.

Crotty P, Sangrey T, Levy WB (2006) Metabolic energy cost of action potential velocity. J Neurophysiol 96:1237–1246.

Dantzler HA, Matott MP, Martinez D, Kline DD (2019) Hydrogen peroxide inhibits neurons in the paraventricular nucleus of the hypothalamus via potassium channel activation. Am J Physiol Regul Integr Comp Physiol 317:R121–R133.

Della Santina L, Inman DM, Lupien CB, Horner PJ, Wong ROL (2013) Differential progression of structural and functional alterations in distinct retinal ganglion cell types in a mouse model of glaucoma. J Neurosci 33:17444–17457.

Denomme N, Lukowski AL, Hull JM, Jameson MB, Bouza AA, Narayan ARH, Isom LL (2020) The voltage-gated sodium channel inhibitor, 4,9-anhydrotetrodotoxin, blocks human Nav1.1 in addition to Nav1.6. Neurosci Lett 724:134853.

Emanuel AJ, Kapur K, Do MTH (2017) Biophysical variation within the M1 type of ganglion cell photoreceptor. Cell Rep 21:1048–1062.

Evans JR, Bielefeldt K (2000) Regulation of sodium currents through oxidation and reduction of thiol residues. Neuroscience 101:229–236.

Fan N, Silverman SM, Liu Y, Wang X, Kim B-J, Tang L, Clark AF, Liu X, Pang I-H (2017) Rapid repeatable in vivo detection of retinal reactive oxygen species. Exp Eye Res 161:71–81.

Felts PA, Yokoyama S, Dib-Hajj S, Black JA, Waxman SG (1997) Sodium channel alpha-subunit mRNAs I, II, III, NaG, Na6 and hNE (PN1): different expression patterns in developing rat nervous system. Brain Res Mol Brain Res 45:71–82.

Fjell J, Dib-Hajj S, Fried K, Black JA, Waxman SG (1997) Differential expression of sodium channel genes in retinal ganglion cells. Brain Res Mol Brain Res 50:197–204.

Fukuda K, Davies SS, Nakajima T, Ong B-H, Kupershmidt S, Fessel J, Amarnath V, Anderson ME, Boyden PA, Viswanathan PC, Roberts LJ, Balser JR (2005) Oxidative mediated lipid peroxidation recapitulates proarrhythmic effects on cardiac sodium channels. Circ Res 97:1262–1269.

Gastaldi M, Bartolomei F, Massacrier A, Planells R, Robaglia-Schlupp A, Cau P (1997) Increase in mRNAs encoding neonatal II and III sodium channel alpha-isoforms during kainate-induced seizures in adult rat hippocampus. Brain Res Mol Brain Res 44:179–190.

Goetz J, Jessen ZF, Jacobi A, Mani A, Cooler S, Greer D, Kadri S, Segal J, Shekhar K, Sanes J, Schwartz GW (2022) Unified classification of mouse retinal ganglion cells using function, morphology, and gene expression. Neuroscience 40:111040.

Griffith TN, Docter TA, Lumpkin EA (2019) Tetrodotoxin-sensitive sodium channels mediate action potential firing and excitability in menthol-sensitive Vglut3-lineage sensory neurons. J Neurosci 39:7086–7101.

Hasenstaub A, Otte S, Callaway E, Sejnowski TJ (2010) Metabolic cost as a unifying principle governing neuronal biophysics. Proc Natl Acad Sci U S A 107:12329–12334.

Kanamori A, Catrinescu M-M, Kanamori N, Mears KA, Beaubien R, Levin LA (2010) Superoxide is an associated signal for apoptosis in axonal injury. Brain 133:2612–2625.

Kassmann M, Hansel A, Leipold E, Birkenbeil J, Lu S-Q, Hoshi T, Heinemann SH (2008) Oxidation of multiple methionine residues impairs rapid sodium channel inactivation. Pflugers Arch 456:1085–1095.

Koch K, McLean J, Berry M, Sterling P, Balasubramanian V, Freed MA (2004) Efficiency of information transmission by retinal ganglion cells. Curr Biol 14:1523–1530.

Koch K, McLean J, Segev R, Freed MA, Berry MJ, Balasubramanian V, Sterling P (2006) How much the eye tells the brain. Curr Biol 16:1428–1434.

Krieger B, Qiao M, Rousso DL, Sanes JR, Meister M (2017) Four alpha ganglion cell types in mouse retina: function, structure, and molecular signatures. PLoS One 12:e0180091.

Lee CR, Patel JC, O'Neill B, Rice ME (2015) Inhibitory and excitatory neuromodulation by hydrogen peroxide: translating energetics to information. J Physiol 593:3431–3446.

Li A, Ségui J, Heinemann SH, Hoshi T (1998) Oxidation regulates cloned neuronal voltage-dependent Ca^{2+} channels expressed in *Xenopus* oocytes. J Neurosci 18:6740–6747.

Lipton SA, Tauck DL (1987) Voltage-dependent conductances of solitary ganglion cells dissociated from the rat retina. J Physiol 385:361–391.

Lukasiewicz P, Werblin F (1988) A slowly inactivating potassium current truncates spike activity in ganglion cells of the tiger salamander retina. J Neurosci 8:4470–4481.

Margolis DJ, Detwiler PB (2007) Different mechanisms generate maintained activity in ON and OFF retinal ganglion cells. J Neurosci 27:5994–6005.

Matynia A, Nguyen E, Sun X, Blixt FW, Parikh S, Kessler J, Pérez de Sevilla Müller L, Habib S, Kim P, Wang ZZ, Rodriguez A, Charles A, Nusinowitz S, Edvinsson L, Barnes S, Brecha NC, Gorin MB (2016) Peripheral Sensory Neurons Expressing Melanopsin Respond to Light. Front Neural Circuits 10:60.

Mojumder DK, Frishman LJ, Otteson DC, Sherry DM (2007) Voltage-gated sodium channel alpha-subunits Na(v)1.1, Na(v)1.2, and Na(v)1.6 in the distal mammalian retina. Mol Vis 13:2163–2182.

O'Brien BJ, Isayama T, Richardson R, Berson DM (2002) Intrinsic physiological properties of cat retinal ganglion cells. J Physiol 538:787–802.

O'Brien BJ, Caldwell JH, Ehring GR, Bumsted O'Brien KM, Luo S, Levinson SR (2008) Tetrodotoxin-resistant voltage-gated sodium channels Na(v) 1.8 and Na(v)1.9 are expressed in the retina. J Comp Neurol 508:940–951.

Ogiwara I, Miyamoto H, Morita N, Atapour N, Mazaki E, Inoue I, Takeuchi T, Itohara S, Yanagawa Y, Obata K, Furuichi T, Hensch TK, Yamakawa K (2007) Nav1.1 localizes to axons of parvalbumin-positive inhibitory interneurons: a circuit basis for epileptic seizures in mice carrying an *Scn1a* gene mutation. J Neurosci 27:5903–5914.

Ohashi M, Hirano T, Watanabe K, Katsumi K, Ohashi N, Baba H, Endo N, Kohno T (2016a) Hydrogen peroxide modulates synaptic transmission in ventral horn neurons of the rat spinal cord. J Physiol 594:115–134.

Ohashi M, Hirano T, Watanabe K, Shoji H, Ohashi N, Baba H, Endo N, Kohno T (2016b) Hydrogen peroxide modulates neuronal excitability and membrane properties in ventral horn neurons of the rat spinal cord. Neuroscience 331:206–220.

Pan Z, Bähring R, Grantyn R, Lipton S (1995) Differential modulation by sulfhydryl redox agents and glutathione of GABA- and glycine-evoked currents in rat retinal ganglion cells. J Neurosci 15:1384–1391.

Peichl L (1991) Alpha ganglion cells in mammalian retinae: common properties, species differences, and some comments on other ganglion cells. Vis Neurosci 7:155–169.

Penna A, Wang D-S, Yu J, Lecker I, Brown PMGE, Bowie D, Orser BA (2014) Hydrogen peroxide increases GABA$_A$ receptor-mediated tonic current in hippocampal neurons. J Neurosci 34:10624–10634.

Perge JA, Koch K, Miller R, Sterling P, Balasubramanian V (2009) How the optic nerve allocates space, energy capacity, and information. J Neurosci 29:7917–7928.

Pilz YL, Bass SJ, Sherman J (2017) A review of mitochondrial optic neuropathies: from inherited to acquired forms. J Optom 10:205–214.

Sakurai K, Chen J, Kefalov VJ (2011) Role of guanylyl cyclase modulation in mouse cone phototransduction. J Neurosci 31:7991–8000.

Sayır F, Kavak S, Meral I, Demir H, Cengiz N, Cobanoğlu U (2013) Effects of crush and axotomy on oxidative stress and some trace element levels in phrenic nerve of rats. Brain Res Bull 92:84–88.

Schlüter F, Leffler A (2016) Oxidation differentially modulates the recombinant voltage-gated Na(+) channel α-subunits Nav1.7 and Nav1.8. Brain Res 1648:127–135.

Smeds L, Takeshita D, Turunen T, Tiihonen J, Westö J, Martyniuk N, Seppänen A, Ala-Laurila P (2019) Paradoxical rules of spike train decoding revealed at the sensitivity limit of vision. Neuron 104:576–587.e11.

Smith BJ, Côté PD, Tremblay F (2017) Contribution of Nav1.8 sodium channels to retinal function. Neuroscience 340:279–290.

Tezel G (2006) Oxidative stress in glaucomatous neurodegeneration: mechanisms and consequences. Prog Retin Eye Res 25:490–513.

Tran NM, Shekhar K, Whitney IE, Jacobi A, Benhar I, Hong G, Yan W, Adiconis X, Arnold ME, Lee JM, Levin JZ, Lin D, Wang C, Lieber CM,

Regev A, He Z, Sanes JR (2019) Single-cell profiles of retinal ganglion cells differing in resilience to injury reveal neuroprotective genes. Neuron 104:1039–1055.e12.

Van Hook MJ, Nawy S, Thoreson WB (2019) Voltage- and calcium-gated ion channels of neurons in the vertebrate retina. Prog Retin Eye Res 72:100760.

Van Wart A, Matthews G (2006) Expression of sodium channels Nav1.2 and Nav1.6 during postnatal development of the retina. Neurosci Lett 403:315–317.

Wang YV, Weick M, Demb JB (2011) Spectral and temporal sensitivity of cone-mediated responses in mouse retinal ganglion cells. J Neurosci 31:7670–7681.

Waxman SG, Kocsis JD, Black JA (1994) Type III sodium channel mRNA is expressed in embryonic but not adult spinal sensory neurons, and is reexpressed following axotomy. J Neurophysiol 72:466–470.

Weick M, Demb JB (2011) Delayed-rectifier K channels contribute to contrast adaptation in mammalian retinal ganglion cells. Neuron 71:166–179.

Werginz P, Raghuram V, Fried SI (2020) Tailoring of the axon initial segment shapes the conversion of synaptic inputs into spiking output in OFF-α T retinal ganglion cells. Sci Adv 6:abb6642.

Wong RCS, Cloherty SL, Ibbotson MR, O'Brien BJ (2012) Intrinsic physiological properties of rat retinal ganglion cells with a comparative analysis. J Neurophysiol 108:2008–2023.

Yu FH, Mantegazza M, Westenbroek RE, Robbins CA, Kalume F, Burton KA, Spain WJ, McKnight GS, Scheuer T, Catterall WA (2006) Reduced sodium current in GABAergic interneurons in a mouse model of severe myoclonic epilepsy in infancy. Nat Neurosci 9:1142–1149.